Calcium Binding Properties of Recombinant Calcium Binding Protein 40, a Major Calcium Binding Protein of Lower Eukaryote *Physarum polycephalum*[†,‡]

Akio Nakamura,[§] Tuyoshi Okagaki,[§] Takashi Takagi,[||] Ken-ichi Nakashima,[⊥] Michio Yazawa,[⊥] and Kazuhiro Kohama*[,§]

Department of Pharmacology, Gunma University School of Medicine, Maebashi, Gunma 371-8511, Japan, Biological Institute, Graduate School of Sciences, Tohoku University, Sendai, Miyagi 980-8578, Japan, and Division of Chemistry, Graduate School of Sciences, Hokkaido University, Sapporo 060-0810, Japan

Received August 9, 1999; Revised Manuscript Received January 3, 2000

ABSTRACT: Calcium binding protein 40 (CBP40) is a Ca^{2+}-binding protein abundant in the plasmodia of *Physarum polycephalum*. CBP40 consists four EF-hand domains in the COOH-terminal half and a putative α-helix domain in the NH_2-terminal half. We expressed recombinant proteins of CBP40 in *Escherichia coli* to investigate its Ca^{2+}-binding properties. Recombinant proteins of CBP40 bound 4 mol of Ca^{2+} with much higher affinity ($pCa_{1/2} = 6.5$) than that of calmodulin. When residues 1−196 of the α-helix domain were deleted, the affinity for Ca^{2+} decreased to $pCa_{1/2} = 4.6$. A chimeric calmodulin was generated by conjugating the α-helix domain of CBP40 with calmodulin. The affinity of Ca^{2+} for the chimeric calmodulin was higher than that for calmodulin, suggesting that the α-helix domain is responsible for the high affinity of CBP40 for Ca^{2+}. CBP40 forms large aggregates reversibly in a Ca^{2+}-dependent manner. A mutant protein with a deletion of NH_2-terminal 32 residues, however, could not aggregate, indicating the importance of these residues for the aggregation. The aggregation occurs above micromolar levels of Ca^{2+} concentration, so it may only occur when CBP40 is secreted out of the plasmodial cells.

The life cycle of the acellular slime mold *Physarum polycephalum* includes microscopic, uninucleated amoebae and macroscopic, multinucleated plasmodia. The mRNA LAV1-2 is expressed specifically in plasmodia (*1*)[1] and the gene is replicated early in S-phase (*2*). LAV1-2 mRNA represents 2.4% of plasmodial mRNA (*1*), indicating that it encodes a major protein. The cDNA for LAV1-2 has been isolated from a plasmodia-specific cDNA library and the nucleotide sequence was determined (*3*). Comparison with protein sequence motifs showed that LAV1-2 contains four EF-hand domains. However, the Ca^{2+}-binding properties of LAV1-2 have not been confirmed biochemically (*4*).

Calmodulin (CaM) is a typical Ca^{2+}-binding protein with four EF-hand motifs. It is known that the affinity of CaM for Ca^{2+} is not very high, being at $pCa_{1/2} = 5$. Interaction with target proteins, such as myosin light-chain kinase, increases its Ca^{2+} affinity sufficiently to explain its physiological relevance (*5*−*7*). Similarly, when CaM formed a complex with mastoparan, it also acquired the higher Ca^{2+} affinity (*8*). The binding of the target proteins or mastoparan to the exposed hydrophobic surfaces in the N- and C-domains of CaM stabilizes the Ca^{2+}-bound state (*5*, *8*−*12*).

However, the affinities for Ca^{2+} of the Ca^{2+}-binding proteins such as neurocalcin δ (*13*), recoverin (*14*, *15*), and BM-40 (*16*) are sufficiently high compared with that of the target-free CaM. In these proteins, it has been suggested that the intramolecular association of the EF-hand domain at the COOH-terminus with the α-helix domain at the NH_2-terminus is important for the high Ca^{2+} affinity.

In this paper, we overexpressed LAV1-2 in *Escherichia coli*, which we termed calcium binding protein 40 (CBP40), purified it, and confirmed its high affinity for Ca^{2+}. We also found that it formed large aggregates in a Ca^{2+}-dependent manner. By producing and characterizing several variants of CBP40, we explored the amino acid sequences responsible for these activities.

MATERIALS AND METHODS

Materials. Plasmodia of *Physarum polycephalum* (strain Ng-1) were grown on Quaker oatmeal (Quaker Oats Company, Chicago, IL) in the dark by the method of Camp (*17*) with some modification (*18*). The migrating sheets of plasmodia were collected and used for experiments.

Chemicals. Ex Taq polymerase, restriction and other modifying enzymes were from Takara Biomedicals (Tokyo,

[†] This work was supported in part by the grants from the Uehara Memorial Foundation, the Smoking Research Foundation, the Special Coordination Funds for Promoting Science and Technology of the Sceince and Technology Agency of the Japan, and Grants-in-Aid for Scientific Research from the Ministry of Education, Science and Culture of Japan.

[‡] The nucleotide sequence of *Physarum* CaM has been submitted to the DDBJ/EMBL/GenBank nucleotide sequence databases under accession number AB022702.

* Correspondence should be addressed to this author at the Department of Pharmacology, Gunma University School of Medicine, Showa-machi 3-39-22, Maebashi, Gunma 371-8511, Japan. E-mail gacho@akagi.sb.gunma-u.ac.jp; Tel +81 272 20 7960; Fax +81 272 20 7966.

[§] Gunma University School of Medicine.

[||] Tohoku University.

[⊥] Hokkaido University.

[1] Abbreviations: CBP40, 40-kDa calcium binding protein; CaM, calmodulin; LB, Luria broth; IPTG, isopropyl 1-thio-β-D-galactopyranoside; MOPS, 3-(*N*-morpholino)propanesulfonic acid; DTT, dithiothreitol; SDS, sodium dodecyl sulfate; PAGE, polyacrylamide gel electrophoresis; BM-40, 40-kDa basement membrane protein.

10.1021/bi991855v CCC: $19.00
Published on Web 03/10/2000

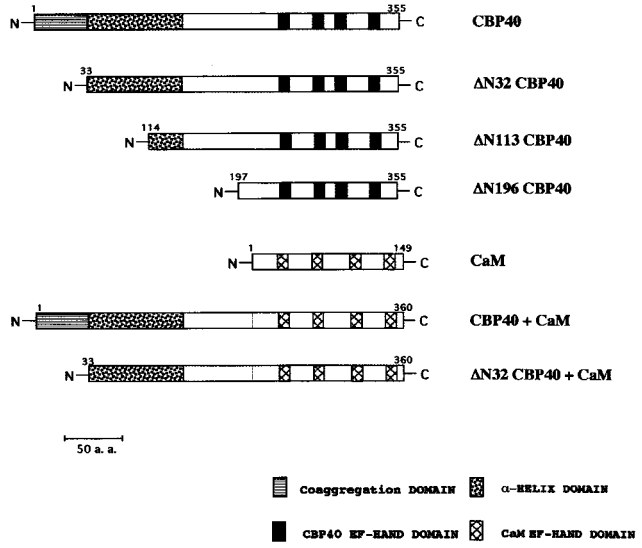

FIGURE 1: Schematic diagram of constructs of CBP40, truncated CBP40, CaM, and chimeric CaMs. The first row indicates a model of the structure of CBP40. CBP40 has distinct sequences at the NH_2-terminal and COOH-terminal halves. The NH_2-terminal half consists of coaggregation domain (hatched bars) and α-helix domain (dotted rectangles). The solid and cross-hatched rectangles indicate the Ca^{2+}-binding loops of EF-hand domains of CBP40 and CaM, respectively. The second row shows the deletion of the coaggregation domain at residues 1−32. The third and fourth rows show the deletions at residues 1−113 and 1−196, respectively. The fifth row shows calmodulin. The sixth and seventh rows show the chimeric proteins between CBP40 and CaM, in which residues 1−211 and 33−211 of N. B. CBP40, respectively, are connected to the NH_2-terminus of CaM. CBP40 and ΔN32CBP40 are recombinant forms of 40 kDa and 38 kDa, respectively, of Ca^{2+}-binding proteins detectable in *Physarum* plasmodia.

Japan), unless otherwise stated. All other chemicals were commercial products of a reagent grade. Solutions were made in MilliQ water (Millipore, Bedford, MA).

PCR Cloning and Protein Engineering. Total RNA from plasmodia was obtained by the AGPC (acid guanidinium−phenol−chloroform) method (*19*) and purified by selective precipitation with 3 M LiCl/6 M urea (*20*). Poly(A)-rich RNA was obtained by using Oligotex-dT30 (Japan Roche, Tokyo, Japan). The first strand of cDNA was synthesized by the method of Krung and Berger (*21*) with avian reverse transcriptase (Life Technologies, MD) and oligo (dT) primer. The remaining RNA was digested with RNase H. The plasmid pLAV1-2 encoding CBP40 was subcloned by PCR based on the reported LAV1-2 nucleotide sequence. The plasmid pCaM encoding *Physarum* calmodulin (CaM) was cloned by the rapid amplification of cDNA ends (*22*) with redundant oligonucleotides based on the already reported amino acid sequence (*3*). The deduced amino acid sequence was in complete agreement with that obtained by peptide mapping (*23*).

The recombinant plasmids related to CBP40, CaM, and deletion mutants were generated by PCR with pLAV1-2 and pCaM (see Figure 1 for their topology). We amplified CBP40 (residues 1−355), ΔN32CBP40 (residues 33−355), ΔN113CBP40 (residues 114−355), ΔN196CBP40 (residues 197−355), and CaM (residues 1−149), in which restriction sites for *Nco*I and *Eco*RI were constructed on either end, and then cloned them into pET21d (Novagen, Madison, WI) via the same two unique restriction sites.

For constructing the chimeras of CBP40 + CaM and ΔN32CBP40 + CaM, the DNA sequences coding residues of 1−211 and 33−211 in CBP40, respectively, were generated by PCR with primers containing additional flanking sequences. Then each PCR product was inserted into the NH_2-terminus of native CaM sequence.

The sequences of each engineered recombinant CBP40 mutant and chimera were confirmed by the dideoxy chain-termination method on an Applied Biosystems model 377 automated DNA sequencer.

Expression and Protein Purification. CBP40 mutants were expressed in *Escherichia coli* BL21(DE3). A 1-L culture of Luria broth (LB) medium containing ampicillin (50 μg mL^{-1}) was grown at 37 °C until the absorbance at 600 nm reached 0.5, when expression was induced with 1 mM isopropyl 1-thio-β-D-galactopyranoside (IPTG). After 3 h, cells were harvested by centrifugation and resuspended in 30 mL of 20 mM Tris (pH 7.5), 50 mM KCl, 25 mM sodium EDTA, 0.1 mM phenylmethanesulfonyl fluoride, and 50 μg/mL pepstatin A (Sigma, St. Louis, MO) and stored at −80 °C. After the suspension was thawed in cold water, bacterial cells were homogenized twice on ice by ultrasonification (Sonifier 200, Branson, Danbury, CT) each for 1 min with a 1-cm tip, 50% cycles, output = 6. The homogenate was ultracentrifuged at 100000*g* for 60 min. The resultant supernatant was subjected to ammonium sulfate fractionation. The mutant proteins were purified from the fraction by column chromatography using a combination of butyl-Toyopearl 650 M and DEAE-Toyopearl 650 M (Tosoh, Tokyo, Japan), and then any minor contaminants were removed by Hiprep Sephacryl HR-200 (Amersham Pharmacia Biotech Inc., Uppsala, Sweden). These columns were incorporated into a model L6200 high-performance liquid chromatography system (Hitachi, Tokyo, Japan).

Calcium Binding Studies. The extent of Ca^{2+} binding was measured by the flow dialysis method with $^{45}CaCl_2$ (DuPont−NEN) in 0.1 M NaCl and 20 mM MOPS/NaOH (pH 7.0) at 25 °C. In some experiments, we add 1 mM dithiothreitol (DTT) or 1 mM $MgCl_2$ to this solution. The method was described in detail by Nakashima et al. (*24*, *25*). The protein concentrations used for the measurement were 40−200 μM. A constant loss of the radioactive ligand intrinsic to our system and the nonspecific Ca^{2+} binding to the flow dialysis apparatus was corrected (*24*, *25*).

We repeated the same experiments several times. Macroscopic dissociation constants for Ca^{2+} of the CBP40 mutants and CaM were obtained by fitting the titration data to the Adair−Klotz multisite-binding equation (*26*) that was modified for the Ca^{2+}-binding data with flow dialysis method (*7*):

$$y = (x/K_1 + 2x^2/K_1K_2 + 3x^3/K_1K_2K_3 + 4x^4/K_1K_2K_3K_4)/$$
$$(1 + x/K_1 + x^2/K_1K_2 + x^3/K_1K_2K_3 + x^4/K_1K_2K_3K_4) + jx$$

where y is the number (mol/mol) of bound Ca^{2+}, x is the concentration of free Ca^{2+}, K_1−K_4 are the macroscopic dissociation constants, and j is the slope term for nonspecific binding (see Table 1). The half-saturating concentration of Ca^{2+} in the titration curve is represented as $pCa_{1/2}$.

Table 1: Ca^{2+} Binding to CBP40 Mutants

	macroscopic dissociation constants (μM)							
	K_1	K_2	K_3	K_4	R^2	$pCa_{1/2}$[b]	Hill	j
ΔN32CBP40	0.0144	0.0961	0.862	6.91	0.991	6.5	0.5	−35.5
ΔN113CBP40	43.69	4.01	0.0438	7.78	0.989	5.7	2.6	−36.8
ΔN196CBP40	4.11	642.3	54.70	0.044	0.995	4.6	2.2	30.3
CaM	2.747	1.338	4.93	5.27	0.957	5.2	1.3	98.9
CBP40 + CaM	0.501	1.89	2.08	0.052	0.980	6.0	1.6	36.6
ΔN32CBP40 + CaM	0.125	4.40	0.229	1.40	0.982	6.1	1.6	−18.8

[a] Each set of macroscopic dissociation constants (micromolar), K_1, K_2, K_3, and K_4, gives the corresponding best-fit curve (shown in Figures 4 and 5) to the Adair−Klotz equation. [b] $pCa_{1/2}$ denotes the half-saturating concentrations of the titration curves. R^2 and Hill refer to the correlation coefficient and Hill coefficient, respectively. j is the slope term for nonspecific binding.

Gel-Permeation-Studies. To examine disulfide bridge in CBP40 and ΔN32CBP40, a Superose 6 prepacked HR 10/30 column (Amersham Pharmacia Biotech Inc., Uppsala, Sweden) was equilibrated in 0.1 M NaCl and 20 mM MOPS/NaOH (pH 7.0) with or without 10 mM DTT, and 100 μL samples were analyzed at 0.4 mL/min. Standards used to calibrate the gel-permeation columns (and their Stokes radii) were thyroglobulin (8.5 nm), apoferritin (6.1 nm), catalase (5.2 nm), aldolase (4.6 nm), bovine serum albumin (3.6 nm), and myoglobin (2.1 nm). The Stokes radius for each protein standard was calculated from references described (*27*, *28*). Distribution coefficients (K_D) were calculated from the elution volume according to the equation $K_D = (V_e - V_0)/(V_t - V_0)$, where V_e is the elution volume of the peak, V_0 is the void volume of the column as determined with blue dextran ($M_r \sim 2 \times 10^6$), and V_t is the total column volume. The Stokes radii (R_s) of CBP40 and ΔN32CBP40 were determined graphically from a linear plot of $(-\log K_D)^{1/2}$ versus R_s for standards in the column.

Cross-Linking Studies. As an alternative examination of disulfide bridge, we subjected CBP40 or ΔN32CBP40 to the chemical cross-linking with BS^3, the activity of which is not affected by the reducing agents (*29*) (Pierce Chemical Co., Rockford, IL). CBP40 or ΔN32CBP40 (10 μM each) in 0.1 M NaCl and 20 mM MOPS/NaOH (pH 7.0) with presence and absence of 10 mM DTT was mixed with 5 mM BS^3 in the final concentration. The mixture was incubated at 25 °C for 2 h. Then, the effects of cross-linking were analyzed by sodium dodecyl sulfate−polyacrylamide gel electrophoresis (SDS−PAGE) (see below).

Detection of Ca^{2+}-Dependent Aggregation. CBP40 or ΔN32CBP40 (10 μM each) dissolved in 0.1 M NaCl and 20 mM MOPS/NaOH (pH 7.0) was mixed with 0.5 mM EGTA or 0.5 mM $CaCl_2$. Then, the mixture was incubated for 30 min at 25 °C, followed by the observation with a dark-field microscope. In some experiments, the concentration of Ca^{2+} was varied in a stepwise manner. To quantify the aggregation, mixtures were centrifuged at 100000*g* for 40 min at 25 °C to precipitate aggregates. The supernatants and precipitates were separately subjected to SDS−PAGE after the precipitates were dissolved with an equal volume of the above buffer.

The reversibility of the aggregation was examined spectrophotometrically. An aliquot of CBP40 at 10 μM in 0.1 M NaCl and 20 mM MOPS/NaOH (pH 7.0) was taken into a quartz semimicro cuvette, and the absorbance at 350 nm was monitored continuously with an Ultrospec 2000 spectrophotometer (Amersham Pharmacia Biotech Inc., Uppsala, Sweden). We detected changes in the absorbance upon adding the concentrated $CaCl_2$ to 0.5 mM in the final concentration followed by chelating Ca^{2+} by 5 mM EDTA. The sample in the cuvette was agitated every 5 min.

Other Procedures. SDS−PAGE was performed as described by Blattler et al. (*30*) using the buffer system of Laemmli (*31*) and the proteins were stained with Coomassie Brilliant Blue. For the quantification of the protein bands, we subjected the gels after SDS−PAGE to a densitometry scanner GT-6500ART (Epson, Tokyo, Japan) connected to a Power Macintosh 6300/120 computer (Apple Japan Inc., Tokyo, Japan) to quantify with NIH image software (version 3.0). Some gels after SDS−PAGE were blotted onto a poly(vinylidene difluoride) membrane (Millipore, Bedford, MA). Bands were excised and sequenced with an Applied Biosystems model 477 automated protein sequencer connected to a model 477A analyzer. All recombinant proteins were more than 95% pure as judged by SDS−PAGE (see Figure 3). Secondary structure predictions including Chou−Fasman program and motif site search were analyzed using the computer programs MacDNASIS Pro 3.6 (Hitachi Software Engineering, San Bruno, CA).

Nucleotide Sequence Accession Number. The nucleotide sequence of *Physarum* CaM has been directly submitted to the DDBJ/EMBL/GenBank nucleotide sequence databases under the accession number AB022702.

RESULTS

Primary Structure of CBP40. CBP40 was a major Ca^{2+}-binding protein in plasmodia of *Physarum polycephalum*, where CBP40 was in two forms of 40 and 38 kDa. The molar ratio of 40 to 38 kDa forms in the plasmodial lysate was 4:1 (data not shown). The 38-kDa peptide was revealed to be a fragment of the 40-kDa peptide missing the NH_2-terminal 32 residues (Met^1−Lys^{32}) by direct amino acid sequencing.

The COOH-terminal half (197−355 residue) of CBP40 contained four EF-hand domains (residues 230−241, 265−276, 295−306, and 322−343). We compared the EF-hand domains of CBP40 with those of CaM (Figure 2) and found little similarity. In CBP40, the dendrogram (Figure 2B) suggests that domains II and IV are most similar, that these two in turn are more similar to domain III, and that domain I is most dissimilar of all. The Gly residue in the middle of the loop of an EF-hand domain is considered important, because the side chain of residues other than Gly may disturb the structure of the motif (*32*). However, in domains II and IV of CBP40, this residue is replaced by Asp^{270} and Lys^{338}, respectively (Figure 2A). In the case of CaM, the 8-residue linker between domain II and III (there are 25 residues

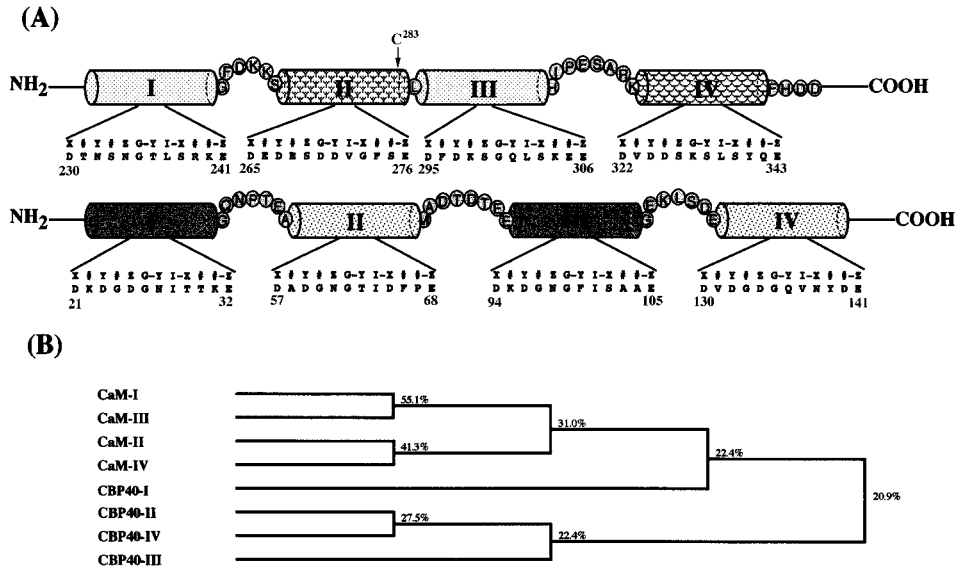

FIGURE 2: Structure of EF-hand domains of *Physarum* CBP40 and CaM. (A) Comparison of four EF-hand domain structure of *Physarum* CBP40 (top) and CaM (bottom). The diagrammatic representation shows EF-hand domain (cylinders) and linker chains of these proteins. The amino acid sequence of the Ca^{2+} binding loop is shown under each EF-hand domain. X, Y, Z and −X, −Y, −Z represent positions of amino acids coordinating to Ca^{2+} in EF-hand domains. # indicates a position where any amino acid is acceptable. (B) Dendrogram of these EF-hand domains in CBP40 and CaM. This dendrogram was generated by progressive alignment UPGMA methods (Mac DNASIS Pro 3.6, Hitachi Software Engineering).

between the domains) forms the handle of a dumbbell-shaped structure and functions as a flexible tether, which was proposed by Persechini and Kretsinger (*33*). The terminal lobes enfold a portion of the target to be activated (*10*−*12*). However, unlike CaM, the corresponding linker in CBP40 is very short, consisting of a single Leu^{285} residue (Figure 2A).

The NH_2-terminal half (residues 1−196) consists of an α-helix-rich region at residues 33−110, which was estimated by Chou−Fasman secondary structure prediction, and contains the RGD sequence at residues 114−116 that is crucial for interaction with its cell surface receptor (*34*). It also contains a consensus sequence (S-G-X-G) for a glycosaminoglycan core domain (*35*, *36*) at residues 166−169. However, the above functions of RGD sequence and S-G-X-G sequence remain to be confirmed with CBP40 by the independent experiments.

Expression of the Wild-Type, Truncated, and Chimeric CBP40s. We constructed recombinant CBP40 to investigate its Ca^{2+}-binding properties. Wild-type and mutant CBP40s were cloned into the high-level expression vector pET21d (*37*). The CBP40 construct contained the open reading frame sequence of LAV1-2. Three truncated CBP40s, ΔN32CBP40, ΔN113CBP40, and ΔN196CBP40, consisting of residues 33−355, 114−355, and 197−355, respectively. In addition, two chimeras in which the NH_2-terminal halves of CBP40 and ΔN32CBP40 were connected to the NH_2-terminus of CaM were also engineered; the resulting constructs are referred to as CBP40 + CaM and ΔN32CBP40 + CaM and are shown schematically in Figure 1.

CBP40 was expressed in *E. coli* strain BL21(DE3), which contains the T7 RNA polymerase gene (*38*). Growth at 37 °C, until an OD_{600} of 0.5 was reached, followed by IPTG induction resulted in a high level of expression of all seven constructs, and average yields were 10−25 mg of protein/L of LB medium. Analysis by SDS−PAGE as shown in Figure 3 confirmed the purity of proteins.

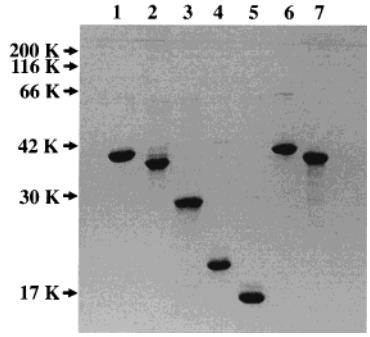

FIGURE 3: Purified recombinant CBP40s and chimeric CaMs. The purity of several mutants was examined by SDS−PAGE. Samples applied to each lane were as follows: CBP40 (lane 1), ΔN32CBP40 (lane 2), ΔN113CBP40 (lane 3), ΔN196CBP40 (lane 4), CaM (lane 5), CBP40 + CaM (lane 6), and ΔN32CBP40 + CaM (lane 7).

Ca^{2+} Binding of Truncated CBP40s. The Ca^{2+}-binding activities of CaM and each of the truncated CBP40s were measured in 0.1 M NaCl and 20 mM MOPS/NaOH (pH 7.0) at 25 °C by the flow dialysis method. The results of Ca^{2+}-binding measurements are summarized in Figure 4, and macroscopic dissociation constants obtained from the best-fit curves satisfying a modified Adair−Klotz equation (see Materials and Methods) are summarized in Table 1. We also examined the Ca^{2+}-binding activity of CaM and ΔN32CBP40, one of the truncated CBP40s (see below), under the above conditions containing 1 mM DTT and 1 mM $MgCl_2$. However, the activity was not altered (data not shown).

We measured Ca^{2+} binding to the EF-hand domain using ΔN196CBP40 (residues 197−355) and found that the maximum Ca^{2+} binding to ΔN196CBP40 was 4 mol/mol. The Ca^{2+}-binding curve showed $pCa_{1/2}$ of 4.6 (Figure 4, closed ◆, and Table 1). The affinity of ΔN196CBP40 for Ca^{2+} was lower than that of CaM with a $pCa_{1/2}$ of 5.2 (Figure 4, ◇, and Table 1). Binding of Ca^{2+} to ΔN196CBP40 was highly cooperative with a Hill coefficient of 2.2.

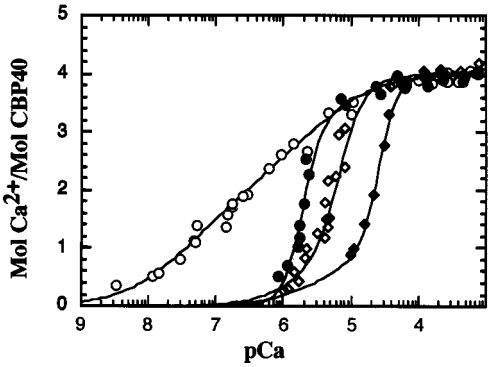

FIGURE 4: Ca^{2+} binding to truncated CBP40s. Ca^{2+} binding was measured by the flow dialysis method with $^{45}CaCl_2$ in 0.1 M NaCl and 20 mM MOPS/NaOH (pH 7.0) at 25 °C. (○) ΔN32CBP40; (●) ΔN113CBP40; (◆) ΔN196CBP40; (◇) CaM. Solid lines show the best-fit curves to the Adair−Klotz equation (eq 1) for each set of data. Parameters for the best-fit curves are summarized in Table 1.

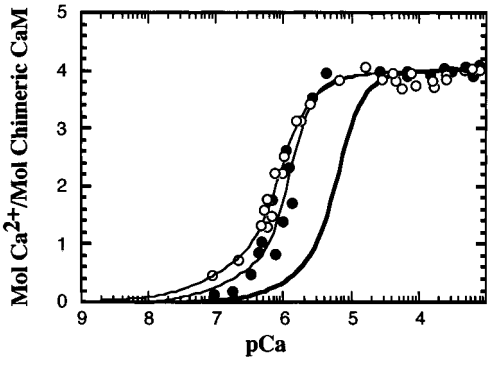

FIGURE 5: Ca^{2+} binding to chimeric CaMs. Ca^{2+} binding experiments were carried out under the same conditions shown in Figure 4. (●) CBP40 + CaM; (○) ΔN32CBP40 + CaM. Curves were generated according to the Adair−Klotz equation with the parameters presented in Table 1. For the purpose of comparison, the Ca^{2+}-binding curve for CaM from Figure 4 is superimposed as a thick solid line.

We measured Ca^{2+} binding to ΔN113CBP40 (residues 114−355) in which a half of the NH_2-terminal domain was linked to ΔN196CBP40. ΔN113CBP40 showed higher affinity for Ca^{2+} than CaM and gave the high Hill coefficient of 2.6 (Table 1 and Figure 4, ●), indicating that the NH_2-terminal domain of 114−196 is responsible for elevating affinity for Ca^{2+}.

Further extension of the NH_2-terminal domain, generating ΔN32CBP40 (residues 33−355, equivalent to the 38-kDa protein found in the plasmodial cell), resulted in a remarkable difference in affinity for Ca^{2+} with a $pCa_{1/2}$ of 6.5 (a 100-fold increase) and apparent negative cooperativity with a Hill coefficient of 0.5 (Figure 4, ○, and Table 1). Thus, the addition of NH_2-terminal domains elevates the affinity for Ca^{2+} by altering the Ca^{2+}-binding properties from the positive to the negative cooperativity. As a result, two high-affinity Ca^{2+} bindings are observed separately from the other two Ca^{2+} bindings.

Unfortunately we could not measure Ca^{2+} binding to parent CBP40, because the measurement was hampered by its Ca^{2+}-dependent aggregation (see below). Therefore, we considered that Ca^{2+} binding to CBP40 should be similar to that of ΔN32CBP40. The rationale will be described in the following section.

Ca^{2+} Binding to Chimeric CaMs. As stated in the previous section, the affinity of CBP40 for Ca^{2+} was increased by fusion of the NH_2-terminal domains. To evaluate the functional contribution of Ca^{2+}-binding sites and the NH_2-terminal domains, two kinds of chimeric CaMs were constructed by adding the NH_2-terminal domains of CBP40 to CaM (Figure 1). The Ca^{2+}-binding activities of two chimeric CaMs are shown in Figure 5 and Table 1. The Ca^{2+}-binding curves of CBP40 + CaM (Figure 5, ●, and Table 1) and ΔN32CBP40 + CaM (Figure 5, ○, and Table 1) showed $pCa_{1/2}$ values of 6.0 and 6.1, respectively, with the same Hill coefficient of 1.6. Thus, no significant differences in the Ca^{2+} affinity and cooperativity are found between these two chimeric CaMs. The affinities of both chimeric CaMs for Ca^{2+} are much higher than that of original CaM (Figure 5, Table 1). This high Ca^{2+} affinity resembles that of ΔN32CBP40. However, unlike ΔN32CBP40, both chimeric CaMs showed positive cooperativity with Hill coefficients of 1.6 in a similar way to original CaM. The molecular mechanism underlying the cooperativity remains to be investigated.

It must be noted again that the Ca^{2+}-binding profiles of both chimeras are not different from each other, although ΔN32CBP40 + CaM lacks the NH_2-terminal 32 residues of CBP40. This result suggests that these residues are not involved in the Ca^{2+}-binding activity of CBP40, giving rationale to our consideration that the Ca^{2+}-binding profile of CBP40 should be the same as that of ΔN32CBP40, which lacks these residues.

Ca^{2+}-Dependent Aggregation of CBP40. CBP40 and ΔN32CBP40 were incubated in the presence or absence of Ca^{2+} and subjected to dark-field microscopic observation (data not shown). In the presence of Ca^{2+}, large structural bodies were observed with CBP40. The minimum dimension was about 10 μm. With ΔN32CBP40, such aggregates were not observed.

We subjected CBP40 to incubation in the presence of various conditions of Ca^{2+} and precipitated the resulting aggregates by centrifugation. The amount of precipitated CBP40 (Figure 6A, ○) increased with the increase in Ca^{2+} concentration. The Ca^{2+}-dependent profile of CBP40 showed a steep rise starting from 1 μM Ca^{2+} and reached the plateau at 100 μM Ca^{2+}. Unlike CBP40, ΔN32CBP40 was not precipitable whether Ca^{2+} was present or not (Figure 6A, ●). Similarly, the fusion proteins of CBP40 + CaM cannot form aggregates in the presence of Ca^{2+} (data not shown).

Under the assumption that Ca^{2+} binding of CBP40 is similar to that of ΔN32CBP40 as described above, CBP40 may have two high-affinity Ca^{2+}-binding sites and two low-affinity Ca^{2+}-binding sites. The high-affinity sites bind Ca^{2+} below the micromolar level of Ca^{2+} concentration but do not form aggregates. Above the micromolar level of Ca^{2+} concentration, where the low-affinity sites bind Ca^{2+}, CBP40 starts to aggregate (Figure 6A).

The reversible nature of aggregation of CBP40 was demonstrated by monitoring the absorbance at 350 nm of CBP40-containing solution (Figure 6B). In the absence of Ca^{2+}, the absorbance remained in the basal level. Upon the addition of Ca^{2+}, it was increased abruptly. Upon the addition of EDTA to chelate Ca^{2+}, we observed a decrease in the absorbance due to the disappearance of the aggregate.

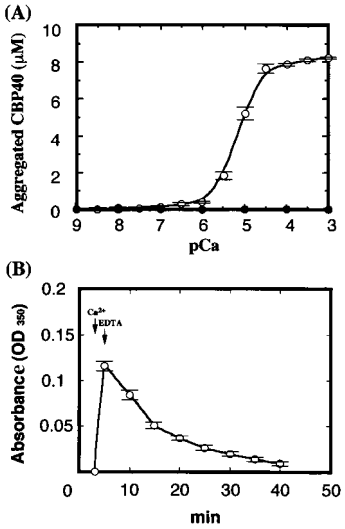

FIGURE 6: Ca^{2+}-dependent aggregation of CBP40. (A) CBP40 (○) or ΔN32CBP40 (●) was incubated for 30 min at 25 °C in 0.1 M NaCl and 20 mM MOPS/NaOH (pH 7.0) with various concentrations of Ca^{2+}. After the incubation, the mixture was subjected to centrifugation. Amounts of precipitates were quantified by SDS−PAGE. The error bars of ΔN32CBP40 are too small to be drawn. (B) Reversibility of aggregation of CBP40. After the aggregation of CBP40 was induced by adding Ca^{2+} (0.5 mM), the aggregates were dispersed by chelating Ca^{2+} by adding EDTA (5 mM). The absorbance at 350 nm was monitored with a spectrophotometer continuously. The error bars are from 6 experiments.

Without additional Ca^{2+}, CBP40 was as soluble as ΔN32CBP40 as shown in Figure 6A. However, they were not monomeric. When CBP40 and ΔN32CBP40 were applied to the gel-filtration column, they were separately eluted (Figure 7B, open circles with double arrows). The Stokes radii of CBP40 and ΔN32CBP40 were 11.4 and 3.6 nm, respectively. Such a large difference is unexpected, when we consider their mobility in SDS−PAGE (Figure 3, lanes 1 and 2).

We subjected CBP40 to cross-linking under comparable conditions for the gel filtration, finding that its mobility was above 200 kDa in SDS−PAGE (Figure 7A, lane 1). However, the cross-linked ΔN32CBP40 showed a mobility of 76 kDa (Figure 7A, lane 3). Thus, CBP40 and ΔN32CBP40 are oligomer and dimer, respectively, in the solution that does not contain Ca^{2+}.

We added DTT to oligomeric CBP40 and dimeric ΔN32CBP40 in the absence of Ca^{2+}, cross-linked, and then subjected the products to SDS−PAGE. They moved as single bands at 40 and 38 kDa (Figure 7A, lanes 2 and 4), respectively, indicating that they disassembled to monomer. We confirmed the monomeric nature under the reduced conditions by the gel-filtration experiment; when CBP40 and ΔN32CBP40 were loaded on the gel-filtration column in the buffer containing DTT, they were eluted at the Stokes radius of 2.7 nm (Figure 7A, × with arrows).

The cross-linking experiments were also carried out in the presence of Ca^{2+}. The cross-linked ΔN32CBP40 moved at 76 kDa in SDS−PAGE, indicating dimeric nature (data not shown). On the other hand, cross-linked CBP40 was absolutely insoluble even in the buffer containing SDS and did not enter the SDS−polyacrylamide gel (data not shown).

In summary, molecular forms of CBP40 and ΔN32CBP40 change depending on their solvent according to Scheme 1.

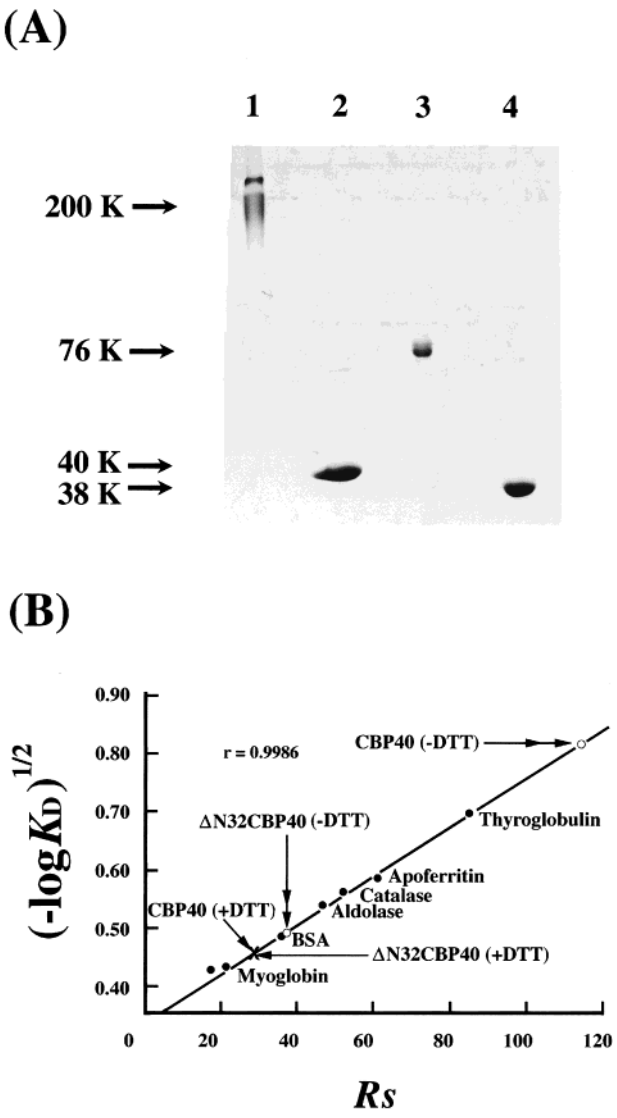

FIGURE 7: Intermolecular disulfide bridge in CBP40 or ΔN32CBP40. (A) Detection by the cross-linking experiment. CBP40 (10 μM) or ΔN32CBP40 (10 μM) were incubated with 5 mM BS^3 at 25 °C for 2 h in the presence or absence of 10 mM DTT, and the proteins were subjected to SDS−PAGE. Samples were treated without (lanes 1 and 3) and with (lanes 2 and 4) DTT; CBP40 (lanes 1 and 2) and ΔN32CBP40 (lanes 3 and 4). (B) Detection with gel-permeation column chromatography. Each samples were applied to Superose 6 columns in the presence or absence of DTT. Arrows, in the presence of DTT; double arrows, in the absence of DTT.

Scheme 1

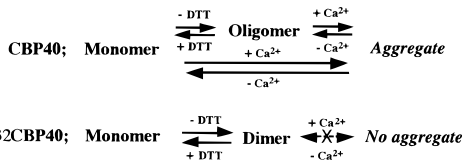

Under the standard conditions in this study, i.e., without additional DTT and Ca^{2+}, CBP40 and ΔN32CBP40 are oligomer and dimer, respectively. The addition of Ca^{2+} at about micromolar concentrations causes CBP40 to form large aggregates. There is a direct path in which CBP40 forms aggregate from monomer, because CBP40 was aggregated by Ca^{2+} even if DTT is present (data not shown). On the other hand, ΔN32CBP40 remains dimeric and does not aggregate even if the Ca^{2+} concentration is increased.

DISCUSSION

The present study reveals that (i) the amino acid sequence of the EF-hand domain of CBP40 is unique when compared with that of other EF-hand proteins; (ii) the α-helix domain (residues 32−196) of ΔN32CBP40 plays an active role in keeping high Ca^{2+}-binding activity of its EF-hand domains; (iii) the Ca^{2+}-binding of CBP40 as examined with ΔN32CBP40 shows apparent negative cooperativity; and (iv) CBP40 forms large aggregates in the presence of Ca^{2+}, for which the NH_2-terminal peptide (residues 1−32) is responsible. We will discuss the molecular mechanisms causing these features and their physiological role in the following.

(1) EF-Hand Structure of CBP40. The superfamily of EF-hand proteins is furnished with E-helix−loop−F-helix structures and makes up the largest Ca^{2+}-binding protein group (*39*). In this group, CaM is the most ubiquitous. The amino acid sequence of CBP40 shows very little similarity to the CaM EF-hand domain. The EF-hand domain of CBP40 is also divergent from those of other EF-hand proteins of lower eukaryotes. It has been argued that EFH5, a Ca^{2+}-binding protein of *Trypanosoma brucei*, is highly homologous to the EF-hand domain of CBP40 (*40*). However, this is not correct, because there is no close relationship between EFH5 and CBP40 when the E-helix−loop−F-helix structures are compared individually (*41*). Thus, the primary structure of the EF-hand domain of CBP40 is unique.

There are several important side chains for coordinating Ca^{2+} by seven oxygen ligands of the E-helix−loop−F-helix structures of the EF-hand superfamily. Above all, a Gly residue in the middle of the loop structure is considered to be important (*32*). The Gly residue is replaced by Asp and Lys in domains II and IV of CBP40, respectively. Therefore, it may be expected that these domains are unable to bind Ca^{2+}. However, CBP40 binds 4 mol of Ca^{2+}/mol (Figure 4), indicating that domains II and IV can indeed bind Ca^{2+}. Since the Ca^{2+}-binding loops in the EF-hand domains of CBP40 show little similarity to those of CaM (Figure 2), this unexpected Ca^{2+} binding may result from some compensating effects of residues in the loop on the unfavorable substitutions for invariant Gly, leading to a more limited range of dihedral angles allowed by these residues.

(2) High Affinity of ΔN32CBP40 for Ca^{2+}. CaM activates several enzymes, such as myosin light-chain kinase, in a Ca^{2+}-dependent manner. A target peptide that binds CaM in the presence of Ca^{2+} has been identified (*42*). The half-saturating concentration of CaM for Ca^{2+} is not very high in itself (*43*), but it is enhanced to the micromolar level when the target peptide is bound (*5*, *6*).

Unlike CaM, the half-saturating concentration of ΔN32CBP40 for Ca^{2+} is at the micromolar level. ΔN32CBP40 is composed of an α-helix domain at the NH_2-terminus and the EF-hand domain at the COOH-terminus (Figure 1). The affinity for Ca^{2+} of the EF-hand domain itself is as low as that of CaM, as was demonstrated by the ΔN196CBP40 construct (Figure 4). The EF-hand domain, however, showed high Ca^{2+} affinity when ligated to the α-helix domain as shown by ΔN32CBP40 (Figure 4). Therefore, the α-helix domain plays an active role in establishing the high Ca^{2+}-affinity of ΔN32CBP40.

The dimeric nature of ΔN32CBP40 was shown by the gel-permeation chromatography (Figure 7B) and the cross-linking experiments (Figure 7A, lane 3). The disulfide bridge was indicated by the experiments that ΔN32CBP40 was divided into monomers when DTT was included as a reducing agent (Figure 7A, lane 4, and Figure 7B). Because Cys^{283} is the sole Cys residue in ΔN32CBP40, we speculate that it forms a dimer by a disulfide bridge between the Cys^{283} residues. The Ca^{2+}-binding activities are not altered whether ΔN32CBP40 forms monomer or not, because they are similar irrespective of the presence of DTT as described in the text. The conserved Ca^{2+}-binding activity is in accordance with the fact that Cys^{283} residue is not included in the Ca^{2+}-binding loop of EF-hand domains as shown at the top of Figure 2A.

There are a few other Ca^{2+}-binding proteins that consist of α-helix and EF-hand domains. They are neurocalcin δ (*13*), recoverin (*14*, *15*), and BM-40 (*16*). The crystal structure of BM-40, recently reported by Hohenester et al. (*16*) revealed the close association of the EF-hand domain with helix A of the α-helix domain. The mode of association has some similarity with the complex of CaM and its target peptide. In both cases, an amphiphilic helix intrudes into hydrophobic core of the EF-hand domain. Such a tight association may stabilize Ca^{2+} bound to EF-hand domain. A similar mechanism can be expected to be responsible for the high Ca^{2+} affinity of ΔN32CBP40.

(3) Physiological Role of CBP40 in Plasmodia. The cytosolic Ca^{2+} concentration is at the 0.1 μM level (*44*) and the extracellular Ca^{2+} concentration should be much higher. Therefore, CBP40 binds Ca^{2+} only at its high-affinity sites in the cell. Ca^{2+} binding at the low-affinity sites occurs only when it is secreted from the cell, where CBP40 should be assembled.

It is known that when the plasmodial vein suffers mechanical wounds, the damaged area is covered by insoluble fibrous material. Recently, CBP40 has been reported to be a substrate for *Physarum* transglutaminase, and the CBP40 may work as a transducer of the signal in response to plasmodial damage (*45*). Therefore, CBP40 may stem the loss of the cytoplasm and repair the damaged area by Ca^{2+}-dependent self-assembly when the cell membrane is broken.

ACKNOWLEDGMENT

We thank Yuki Hanyuda and Yukie Roppongi for their excellent technical assistance.

REFERENCES

1. Pallotta, D., Laroche A., Tessier, A., Schinnick, T., and Lemieux, G. (1986) *Biochem. Cell Biol. 64*, 1294−1302.
2. Pierron, G., Benard, M., Puvion, E., Flanagan, R., Sauer, H. W., and Pallotta, D. (1989) *Nucleic Acids Res. 17*, 553−566.
3. Laroche, A., Lemieux, G., and Pallota, D. (1989) *Nucleic Acids Res. 17*, 10502.
4. Nakayama, S., and Kretsinger, R. H. (1994) *Annu. Rev. Biophys. Biomol. Struct. 23*, 473−507.
5. Olwin, B. B., Edelman, A. M., Krebs, E. G., and Storm, D. R. (1984) *J. Biol. Chem. 259*, 10949−10955.
6. Olwin, B. B., and Storm, D. R. (1985) *Biochemistry 24*, 8081−8066.
7. Stemmer, P. M., and Klee, C. B. (1994) *Biochemistry 33*, 6859−6866.
8. Yazawa, M., Ikura, M., Hikichi, K., Ying, L., and Yagi, K. (1987) *J. Biol. Chem. 262*, 10951−10954.
9. Babu, Y. S., Bugg, C. E., and Cook, W. J. (1988) *J. Mol. Biol. 204*, 191−204.

10. Ikura, M., Clore, G. M., Gronenborn, A. M., Zhu, G., Klee, C. B., and Bax, A .(1992) *Science 256*, 632−638.
11. Meador, W. E., Means, A. R., and Quiocho, F. A. (1992) *Science 257*, 1251−1255.
12. Meador, W. E., Means, A. R., and Quiocho, F. A. (1993) *Science 262*, 1718−11721.
13. Ladan, D. (1995) *J. Biol. Chem. 270*, 3179−3185.
14. Dizhoor, A. M., Chen, C. K., Olshevskaya, E., Sinelnikova, V. V., Phillipov, P., and Hurley, J. B. (1993) *Science 259*, 829−832.
15. Zozulya, S., and Stryer, L. (1992) *Proc. Natl. Acad. Sci. U.S.A. 89*, 11569−11573.
16. Hohenester, E., Maurer, P., Hohenadl, C., Timpl, R., Jansonius, J. N., and Engel, J. (1996) *Nat. Struct. Biol. 3*, 67−73.
17. Camp, W. G. (1936) *Bull. Torrey Bolt. Club 63*, 205−210.
18. Hatano, S., and Oosawa, F. (1966) *Biochim. Biophys. Acta 127*, 488−498.
19. Chomczynski, P., and Sacchi, N. (1987) *Anal. Biochem. 162*, 156−159.
20. Auffray, C., and Rougeon, F. (1980) *Eur. J. Biochem. 107*, 303−314.
21. Krung, M. S., and Berger, S. L. (1987) *Methods Enzymol. 152*, 316−325.
22. Frohman, M. A., Dush, M. K., and Martin, G. R. (1988) *Proc. Natl. Acad. Sci. U.S.A. 85*, 8998−9002.
23. Toda, H., Okagaki, T., and Kohama, K. (1990) in *Advances in second messenger and phosphoprotein research* (Nishizuka, Y., Endo, M., and Tanaka, T., Eds.) Vol. 24, p 614, Raven Press, New York.
24. Nakashima, K., Maekawa, H., and Yazawa, M. (1996) *Biochemistry 35*, 5602−5610.
25. Nakashima, K., Ishida, H., Ohki, S., Hikichi, K., and Yazawa, M. (1999) *Biochemistry 38*, 98−104.
26. Edsall, J. T., and Wymann, J. (1958) in *Biophysical Chemistry*, Vol. 1, pp 591−662, Academic Press, New York.
27. Seigel, L. M., and Monty, K. J. (1966) *Biochim. Biophys. Acta 112*, 346−362.
28. Uversky, V. N. (1993) *Biochemistry 32*, 13288−13298.
29. Markovic, I., Pulyaeva, H., Sokoloff, A., and Chernomordik, L. V. (1998) *J. Cell Biol. 143*, 1155−1166.
30. Blattler, D. P., Garner, F., Van Slyke, K., and Bradley, A. (1972) *J. Chromatogr. 64*, 147−155.
31. Laemmli, U. K. (1970) *Nature 227*, 680−685.
32. Kretsinger, R. H. (1980) *CRC Crit. Rev. Biochem. 8*, 119−174.
33. Persechini, A., and Kretsinger, R. H. (1988) *J. Biol. Chem. 263*, 12175−12178.
34. Ruoslahti, E., and Pierschbacher, M. D. (1986) *Cell 44*, 517−518.
35. Bourdon, M. A., Krusius, T., Campbell, S., Schwartz, N. B., and Ruoslahti, E. (1987) *Proc. Natl. Acad. Sci. U.S.A. 84*, 3194−3198.
36. Hassell, J. R., Kimura, J. H., and Hascall, V. C. (1986) *Annu. Rev. Biochem. 55*, 539−567.
37. Tabor, S., and Richardson, C. C. (1985) *Proc. Natl. Acad. Sci. U.S.A. 82*, 1074−1078.
38. Studier, F. W., and Moffatt, B. A. (1986) *J. Mol. Biol. 189*, 113−130.
39. Kretsinger, R. H., and Nockolds, C. E. (1973) *J. Biol. Chem. 248*, 3313−3326.
40. Moncrief, N. D., Kretsinger, R. H., and Goodman, M. (1990) *J. Mol. Evol. 30*, 522−562.
41. Wong, S., Kretsinger, R. H., and Campbell, D. A. (1992) *Mol. Gen. Genet. 233*, 225−230.
42. Blumenthal, D. K., Takio, K., Edelman, A. M., Charbonneau, H., Titani, K., Walsh, K. A., and Krebs, E. G. (1985) *Proc. Natl. Acad. Sci. U.S.A. 82*, 3187−3191.
43. Crouch, T. H., and Klee, C. B. (1980) *Biochemistry 19*, 3692−3698.
44. Ridgway, E. B., and Durham, A. C. (1976) *J. Cell Biol. 69*, 223−226.
45. Mottahedeh, J., and Marsh, R. (1998) *J. Biol. Chem. 273*, 29888−29895.

BI991855V